Direct Evidence of Intervalence Charge-Transfer States of Eu-Doped Luminescent Materials

Jonas J. Joos[1], Luis Seijo[2], Zoila Barandiarán[2]

[1]LumiLab, Department of Solid State Sciences, Ghent University, Krijgslaan 281-S1, 9000 Gent, Belgium. Center for Nano- and Biophotonics (NB Photonics), Ghent University, Belgium

[2]Departamento de Química, Instituto Universitario de Ciencia de Materiales Nicolás Cabrera, and Condensed Matter Physics Center (IFIMAC), Universidad Autónoma de Madrid, 28049 Madrid, Spain

This paper was published in Phys. Chem. Lett. (Available online 18 March 2019)

This version is the unedited, accepted version after peer review.

The edited version can be found at:

https://pubs.acs.org/doi/10.1021/acs.jpclett.9b00342

THE JOURNAL OF PHYSICAL CHEMISTRY Letters

Letter

Cite This: J. Phys. Chem. Lett. 2019, 10, 1581−1586

pubs.acs.org/JPCL

Direct Evidence of Intervalence Charge-Transfer States of Eu-Doped Luminescent Materials

Jonas J. Joos,*[,†] Luis Seijo,[‡] and Zoila Barandiarán[‡]

[†]LumiLab, Department of Solid State Sciences, and Center for Nano- and Biophotonics (NB-Photonics), Ghent University, 9000 Ghent, Belgium

[‡]Departamento de Química, Instituto Universitario de Ciencia de Materiales Nicolás Cabrera, and Condensed Matter Physics Center (IFIMAC), Universidad Autónoma de Madrid, 28049 Madrid, Spain

Direct Evidence of Intervalence Charge Transfer States of Eu-doped Luminescent Materials

Jonas J. Joos,*,† Luis Seijo,‡ and Zoila Barandiarán‡

†*LumiLab, Department of Solid State Sciences, and Center for Nano- and Biophotonics (NB-Photonics), Ghent University, 9000 Ghent, Belgium*
‡*Departamento de Química, Instituto Universitario de Ciencia de Materiales Nicolás Cabrera, and Condensed Matter Physics Center (IFIMAC), Universidad Autónoma de Madrid, 28049 Madrid, Spain*

E-mail: jonas.joos@ugent.be

Abstract

Direct evidence is given for the existence of intervalence charge transfer (IVCT) states of Eu^{2+}/Eu^{3+} pairs in Eu-doped CaF_2, SrF_2, and BaF_2. They are detected in diffuse reflectance spectra. In doped materials, IVCT states, in which an electron transfer occurs between two metal sites differing only in oxidation state, are rather difficult to observe because the absorption bands are extremely broad and flat, their intensity is low, and no emission follows the IVCT absorptions. Their assignment as IVCT states is provided by state-of-the-art multiconfigurational *ab initio* calculations. Although IVCT states of lanthanide-doped materials have largely been overlooked so far, they can cause luminescence quenching and even complete luminescence excitation loss. Their direct observation and independent assignment in classical dopant (Eu) and hosts (CaF_2, SrF_2, BaF_2) is very significant: it suggests that the occurrence of IVCT states in other lanthanide-activated materials is very likely overlooked and their impact ignored.

Graphical TOC Entry

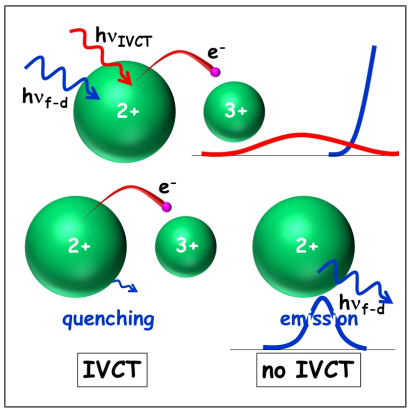

Keywords

Intervalence charge transfer, IVCT, Eu, fluoride crystals, luminescence quenching

Intervalence charge transfer (IVCT, electron transfer between two metal sites differing only in oxidation state[1]) in lanthanide containing materials has received very little attention compared to the vast amount of work focused on transition metal compounds.[2–4] In mixed valence lanthanide materials, where a certain lanthanide ion occurs with different oxidation states, most of the work has addressed thermally induced electron hopping between the centers of mixed valence pairs; the pioneering work of Berkooz *et al.*[5] in Eu_3S_4 is a prototype in this area. Work on photoinduced intervalence electron transfer is very scarce: The reports by Wickleder of Eu^{2+}/Eu^{3+} IVCT absorption bands in the mixed valence Eu chloride crystals $Na_5Eu_7Cl_{22}$ and KEu_2Cl_6 are exceptional and significant.[6,7] In doped materials, where lanthanide ions are diluted in a crystalline host, the only identification of an IVCT absorption is the tentative assignment of a broad band in the reflection spectrum of Ce-doped $LaPO_4$ as a Ce^{3+}/Ce^{4+} IVCT absorption by van Schaik *et al.*,[8] as far as we know.

Regardless of its absence in literature, the presence of dopant pairs or clusters of mixed valence and hence the occurrence of IVCT transitions are expected to have an important impact on the performance of luminescent materials. In applications, such as white light-emitting diodes for lighting or displays, a high luminescence quantum efficiency and a limited thermal quenching are required.[9] It is generally accepted that the presence of defects in close proximity to the luminescence activator can deteriorate the latter's properties,[10] either by directly generating nonradiative decay paths[11–13] or by capturing charge-carriers from the activator, retarding or quenching the luminescence.[14–16] Here, the undesired defect under investigation is a metal ion emanating from the same chemical element than the luminescence activator, but differing in oxidation state.

The IVCT states arise naturally in the electronic structure of the metal pair and represent an electron transfer between both centers, symbolically written as M^{n+}–$M^{(n+1)+} \rightarrow M^{(n+1)+}$–$M^{n+}$.[17] Both ground and excited states of the individual ions can take part in an IVCT and the so called IVCT energy diagrams allow to read single-valence and IVCT transitions and crossings (see Fig. 1).

IVCT states produce extremely broad and flat absorption bands due to the large offset between the respective potential energy surfaces (Fig. 1, left), which is related to the stressed geometry obtained after the electron transfer. Indeed, typical ionic radii differ substantially between oxidation states, e.g. 1.25 pm versus 1.07 pm for Eu^{2+} and Eu^{3+} in 8-fold coordination respectively.[18] Furthermore, IVCT absorption is not followed by any emission because the absorbed energy is immediately nonradiatively dissipated by multiphonon relaxation (Fig. 1, left). These characteristics complicate the observation of IVCT states, explaining their absence in literature.

Concerning the effect of IVCT states on regular luminescent levels, two scenarios can be distinguished when a structurally stressed IVCT state is close in energy to a potentially luminescent level of one of the mixed valence centers: the IVCT state is below the luminescent level (case A) or above it (case B) (cf. Fig. 1 A and B). This may result in luminescence quenching in case A, where the crossing between both levels gives rise to an energy barrier for quenching, or luminescence excitation loss in case B, where no energy barrier occurs and a full structural relaxation can proceed spontaneously, even at low temperature. When the stressed IVCT state is far in energy from an emitting level, the luminescence is not expected to be quenched, although additional absorption and emission bands can occur.

Indeed, IVCT luminescence has recently been invoked to interpret the anomalous emissions of Ce-doped elpasolites and Yb-doped fluorides,[19,20] as well as the laser-induced white emission from Ce in Sr_2CeO_4.[21] Experimental evidence has shown that the anomalous emission of CaF_2:Yb is not due to impurity-trapped-excitons, which was the accepted model during three decades, and the complexity inherent in the mixed valence nature of Yb in fluorite has been demonstrated.[22,23]

All this points out the importance of provid-

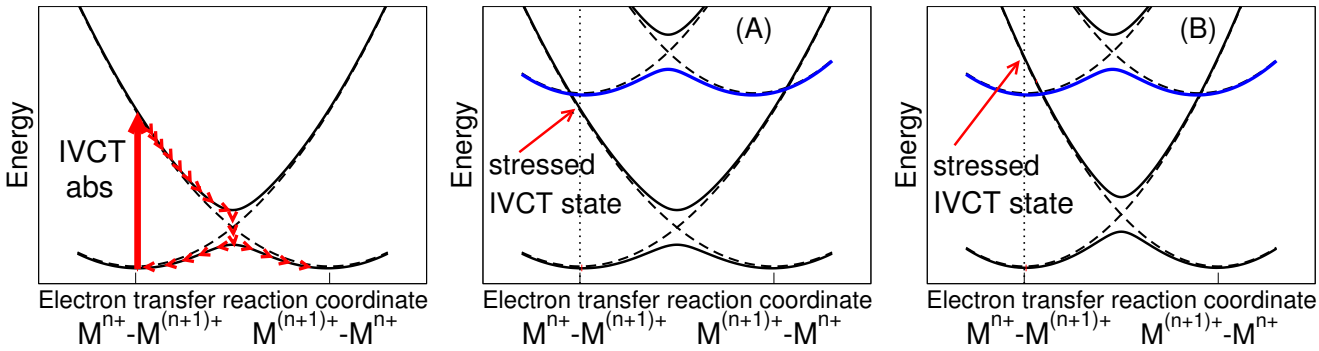

Figure 1: Schematic representation of an intervalence charge transfer (IVCT) absorption (red arrow) followed by nonradiative decay (left). A structurally stressed IVCT state is close and below (A) or close and above (B) a potentially luminescent level (in blue); this may result in luminescence quenching (A) or luminescence excitation loss (B).

ing direct evidence of the occurrence of intervalence charge transfer states in lanthanide-doped materials, which is still missing.

Here, we show direct evidence of IVCT states of Eu in fluoride hosts by combining diffuse reflectance spectroscopy and state-of-the-art multiconfigurational *ab initio* calculations. This evidence points out the importance of investigating the role of IVCT in the luminescence of lanthanide-doped materials.

In the series of Eu-doped CaF_2, SrF_2, and BaF_2 samples studied here, a broad and flat absorption band is identified as an $Eu^{2+}4f \rightarrow Eu^{3+}4f$ IVCT transition. A host driven energy shift of the IVCT absorption band to higher energies, towards the low-energy edge of the Eu^{2+} $4f$–$5d$ absorption spectrum, is observed. So, the IVCT and $4f$–$5d$ absorption bands are well separated in CaF_2:Eu, get closer in SrF_2:Eu, and overlap significantly in BaF_2:Eu (case A). The crossings between the stressed IVCT states and the excited $Eu^{2+}4f^65d$ states in BaF_2:Eu provide a nonradiative decay channel to the relaxed mixed valence ground state and an explanation to the fact that the blue Eu^{2+} $5d$–$4f$ emission observed in CaF_2 and SrF_2, is quenched in BaF_2.[24]

The results of the quantum mechanical calculations of the diabatic IVCT energy diagrams are presented in the upper panels of Fig. 2 and in Table 1. All levels of the Eu^{2+}/Eu^{3+} mixed valence pairs corresponding to the ground multiplets are plotted in violet, i.e. the $[4f^7(^8S_{7/2}),4f^6(^7F_J)]$ levels of the Eu^{2+}–Eu^{3+} configuration of the pair (left parabolas) and the $[4f^6(^7F_J),4f^7(^8S_{7/2})]$ levels of the Eu^{3+}–Eu^{2+} configuration of the pair (right parabolas), which are all abbreviated as $Eu^{2+}(^8S_{7/2})/Eu^{3+}(^7F_J)$. The levels that correspond to the second $4f^6$ multiplet of Eu^{3+} are in orange: $Eu^{2+}(^8S_{7/2})/Eu^{3+}(^5D_J)$. And the very dense bottom of the lowest $Eu^{2+}4f^65de_g$ manifold is plotted in blue: $Eu^{2+}4f^6(^7F_J)5de_g/Eu^{3+}(^7F_J)$. In the calculations, we assumed that Eu^{3+} is non-locally compensated and, in consequence, the IVCT diagram is symmetric. Therefore, it is sufficient to use one side of the diagram (e.g. the left hand side, with electron transfer reaction coordinate $Q_{et}<0$) to read the vertical transition energies that lead to the absorption spectra.

From the Eu^{2+}–Eu^{3+} ground state minimum, $[^8S_{7/2},^7F_J]$ (cf. its structure in Table 1), a set of vertical IVCT absorptions are found that reach all the stressed crystal components of Eu^{3+}–Eu^{2+} $[^7F_J,^8S_{7/2}]$ as indicated by green arrows in Fig. 2 (upper panels). These are photoinduced $Eu^{2+}4f^7$–to–$Eu^{3+}4f^6$ electron transfer transitions. The IVCT states reached vertically are structurally very stressed, hence the corresponding absorption bands are very broad; their calculated peak energies are given in Table 1. The peak energies span wide intervals: 15100–

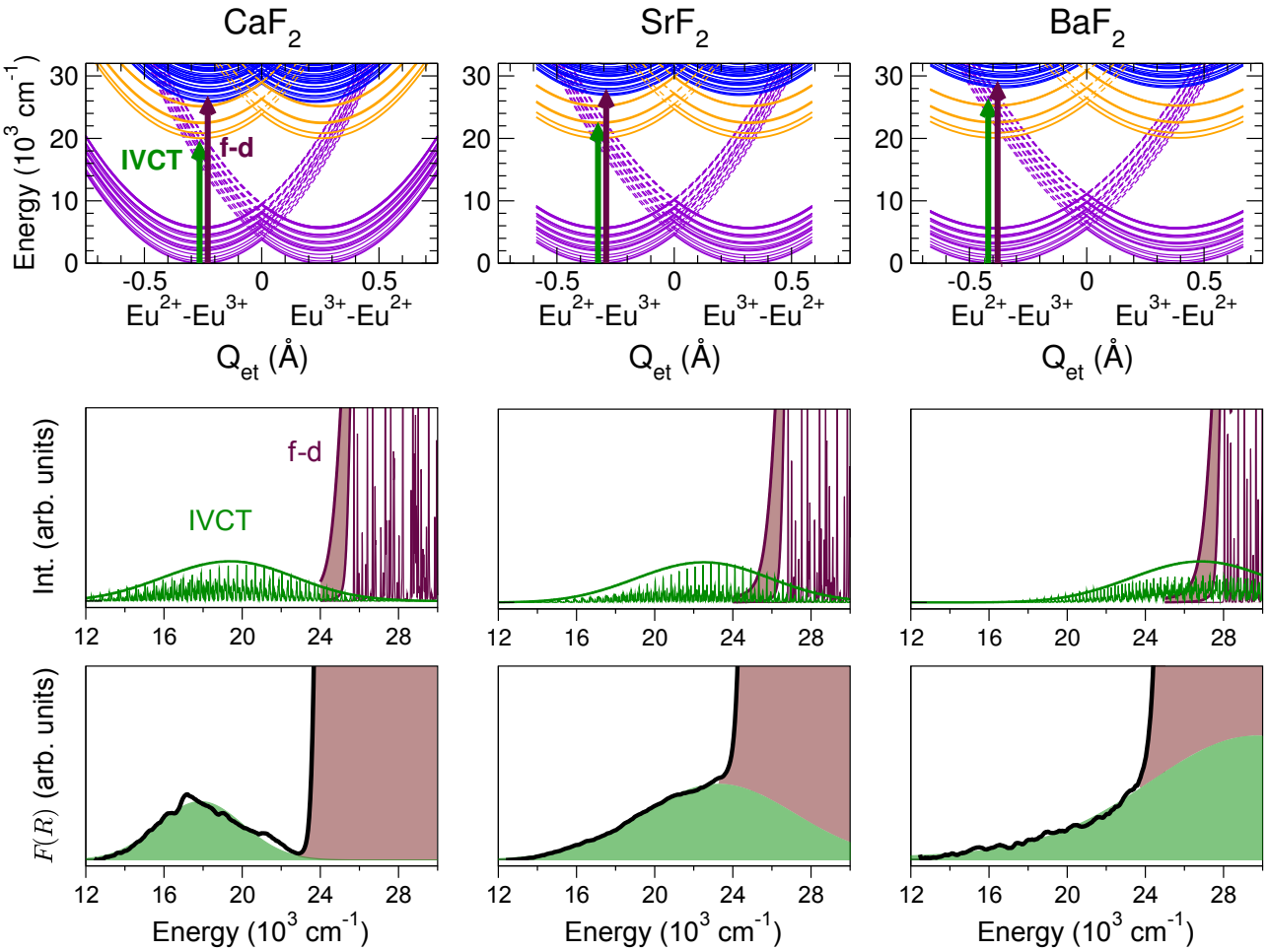

Figure 2: Theoretical and experimental results for Eu-doped CaF_2, SrF_2, and BaF_2. Top: Diabatic Eu^{2+}/Eu^{3+} IVCT configurational energy diagrams computed using the results of *ab initio* calculations. $Eu^{2+}(^8S_{7/2})/Eu^{3+}(^7F_J)$ (violet), $Eu^{2+}(^8S_{7/2})/Eu^{3+}(^5D_J)$ (orange), and $Eu^{2+}4f^6(^7F_J)5de_g/Eu^{3+}(^7F_J)$ (blue) states are plotted. Middle: Theoretical absorption spectra. $Eu^{2+}4f^7 \rightarrow Eu^{3+}4f^6$ IVCT absorption bands in green; low energy edge of Eu^{2+} $4f^7 \rightarrow 4f^6(^7F_J)5de_g$ absorptions in brown. Bottom: Experimental absorption spectra (black lines) obtained by transforming diffuse reflectance spectra by means of the Kubelka-Munk prescription; the green filled area is the result of a fit.

20800 cm^{-1} (CaF_2); 18200–23900 cm^{-1} (SrF_2); and 22000–27700 cm^{-1} (BaF_2). The superpositions of all the IVCT transitions lead to the very broad IVCT absorption envelopes plotted in green in Fig. 2 (middle panels) with higher and lower resolutions; peak energies and full width at half maximum (FWHM) values aregiven in Table 1; the relative heights of the IVCT and $4f-5d$ bands are arbitrary.

A host driven shift of the IVCT band towards higher energies is evident. This shift is caused by the increase of the mismatch between the Eu^{2+}-$F^-$and Eu^{3+}-F^-bond lengths across the CaF_2 - SrF_2 - BaF_2 series. In effect, this mismatch is directly related to the horizontal offset between the two equivalent minima in the electron transfer reaction coordinate $[\Delta Q_{et,e} \approx 4(d_{Eu^{2+}-F^-} - d_{Eu^{3+}-F^-})]$[17,20] and the increase of $\Delta Q_{et,e}$ from 0.512 Å (CaF_2) to 0.632 Å (SrF_2) to 0.782 Å (BaF_2) produces an associated increase of the IVCT peak energy, which is only slightly compensated by the decrease of the EuF_8 breathing mode vibrational frequencies across the series.

The host driven shift brings the IVCT absorption bands closer to the bottom of the Eu^{2+} $4f$–$5d$ band (cf. Table 1 and Fig. 2, middle panel, brown envelope). The IVCT and $4f$–$5d$ bands are well separated in CaF_2, get closer in SrF_2, and overlap significantly in

BaF_2. In effect, as the horizontal offset increases, the branches of stressed Eu^{3+}-Eu^{2+} $[^7F_J, ^8S_{7/2}]$ IVCT states get closer to the bottom of the Eu^{2+}-Eu^{3+} $[4f^6(^7F_J)5de_g, ^7F_J]$ manifold, causing the absorption bands to overlap and enabling non-radiative decay through electron transfer crossings. In Table 1 the energy barriers for IVCT non-radiative decay show a clear trend from CaF_2 to SrF_2 to BaF_2: 797 cm^{-1}, 374 cm^{-1}, 95 cm^{-1}, which is significant in spite of the diabatic approximation; adiabatic avoided crossings could decrease their values, but would keep their trend in the host series, hence Eu^{2+} $4f^6(^7F_J)5de_g$ luminescence quenching should be expected in BaF_2.

Diffuse reflectance spectroscopy on in-house synthesized polycrystalline powders is employed in the search for the absorption bands that are predicted by the quantum mechanical calculations. Fluorides, doped with 1% of Eu were selected for these experiments. This is a doping concentration which is representative for most applications, including LED phosphors, and which is still sufficiently low to avoid the formation of Eu aggregates.[25] Figure 3 shows the low energy part of the resulting spectra for the alkaline earth fluorides, each doped with 1% of Eu. The spectra are dominated by the $4f^7 \rightarrow 4f^6 5d^1$ band of Eu^{2+} in accordance to the well-known absorption and excitation spectra of Eu^{2+} in the fluorides.[24,26,27] By carefully inspecting the lower-energy part of the reflection spectra, a rather weak absorption band is indeed found in addition, partly overlapping

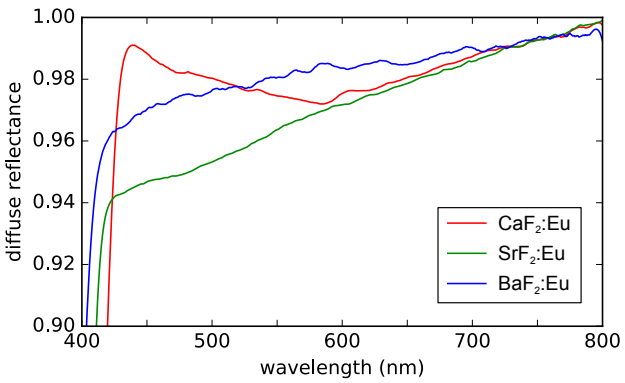

Figure 3: Diffuse reflectance spectra for CaF_2, SrF_2 and BaF_2 powders, all doped with 1% of Eu. Measured at room temperature.

Table 1: Vertical electronic transition energies calculated at the fixed Eu–F equilibrium distances of the initial $Eu^{2+}(^8S_{7/2})$ – $Eu^{3+}(1\ A_{1g})$ ground states. Selected diabatic energy barriers and Eu-F distance in the left and right moieties. Energies and vibrational frequencies in cm^{-1}; distances in Å.

				CaF_2	SrF_2	BaF_2
Eu-F equilibrium distances						
$Eu^{2+}(^8S_{7/2})$				2.388	2.470	2.558
$Eu^{3+}(1\ A_{1g})$				2.261	2.313	2.363
difference				0.127	0.157	0.195
Equilibrium Q_{et}				-0.256	-0.316	-0.391
EuF_8 breathing mode vibrational frequencies						
$Eu^{2+}(^8S_{7/2})$				423	370	321
$Eu^{3+}(1\ A_{1g})$				495	445	402
mean values				459	408	362
Vertical IVCT absorptions						
Eu^{2+}	Eu^{3+} →	Eu^{3+}	Eu^{2+}			
$4f^7$	$4f^6$	$4f^6$	$4f^7$			
$^8S_{7/2}$	$1\ A_{1g}$	$1\ A_{1g}$	$^8S_{7/2}$	15117	18191	22019
		$1\ T_{1g}$		15482	18562	22392
		$1\ T_{2g}$		16035	19145	22999
		$1\ E_g$		16394	19432	23229
		$2\ T_{1g}$		17097	20180	24014
		$2\ T_{2g}$		17160	20223	24043
		$1\ A_{2g}$		17337	20372	24168
		$2\ A_{1g}$		17776	20921	24808
		$3\ T_{1g}$		18182	21253	25080
		$3\ T_{2g}$		18372	21421	25224
		$2\ E_g$		18445	21473	25264
		$4\ T_{2g}$		19241	22329	26171
		$4\ T_{1g}$		19432	22485	26300
		$3\ E_g$		19589	22627	26423
		$5\ T_{1g}$		19590	22627	26423
		$3\ A_{1g}$		20586	23652	27477
		$6\ T_{1g}$		20626	23686	27506
		$5\ T_{2g}$		20645	23706	27524
		$4\ E_g$		20807	23851	27652
		$6\ T_{2g}$		20811	23854	27654
		$2\ A_{2g}$		20820	23860	27659
Simulated IVCT absorption band						
band maxima				19300	22500	26600
FWHM				7800	8000	8200
Lowest Eu^{2+} $4f^7 - 4f^6 5d$ absorption						
Eu^{2+}	Eu^{3+} →	Eu^{2+}	Eu^{3+}			
$^8S_{7/2}$	$1\ A_{1g}$	$1\ \Gamma_{8g}$	$1\ A_{1g}$	25800	26900	28200
Diabatic energy barriers for non-radiative decay:						
Eu^{2+}	Eu^{3+} ⇝	Eu^{3+}	Eu^{2+}			
$1\ \Gamma_{8g}$	$1\ A_{1g}$	$2\ A_{2g}$	$^8S_{7/2}$	797	374	95
Eu-F distance at left center (d_L):				2.403	2.476	2.549
Eu-F distance at right center (d_R):				2.233	2.293	2.351

with the $4f^7 \rightarrow 4f^6 5d^1$ band and extending up to 800 nm (12500 cm^{-1}) on the low-energy side. Because of the low absorption strength of these low-energy bands, diffuse reflectance spectroscopy requires a white baseline obtained from undoped fluorides. These underwent the same thermal treatment as the doped samples,

ensuring that only absorption features due to the presence of Eu are measured (Fig. 3).

The qualitative characteristics of the low-energy absorption bands correspond to the computed characteristics for IVCT absorptions, i.e. a broad band that is blue-shifted from CaF_2 to SrF_2 to BaF_2, approaching the on-set of the Eu^{2+} $4f-5d$ absorptions. In order to allow for a better comparison, the diffuse reflectance spectra are transformed to units of absorption by means of the Kubelka-Munk prescription, $F(R)$.[28,29] The result is shown in Fig. 2 (bottom panel). Notwithstanding the approximate character of Kubelka-Munk theory,[29,30] the obtained spectra are strikingly similar to the simulated spectra. A very similar absorption band was measured in BaF_2:Eu by Moine *et al.*[27] At that time, it was attributed to an impurity trapped exciton, an explanation that now loses credibility. No impurity trapped excitons are found in the low-energy region of the BaF_2:Eu electronic structures, and this band fits perfectly in the proposed IVCT model.

The IVCT absorption band was fitted with a Voigt spectral profile,[31] allowing a rough estimation of its position and its width (cf. green filled area in Fig. 2 (bottom panel) and Table 2). The correspondence between computed and experimental band positions is remarkable, of the order of 2000 cm^{-1}, indicating further the correctness of the IVCT assignment. Similarity with IVCT absorptions identified in mixed valence Eu chloride crystals, reinforces this theoretical assignment.[6,7]

In Table 2 we also report the absorption strengths of the IVCT bands relative to the $4f^7 \rightarrow 4f^6(^7F_J)5de_g$ bands. The IVCT absorptions are much weaker. They are also of the same order of magnitude in all cases, although, in principle, we do not expect a very stable value for the intensity of an IVCT absorption band in these mixed valence doped materials, because it is a very complex property that depends on the actual distribution of Eu^{2+} and Eu^{3+} ions across the samples: It depends on the distribution of concentrations of Eu^{2+}/Eu^{3+} pairs with different Eu^{2+}-Eu^{3+} distance (since the oscillator strength is distance dependent), which depends in turn on the doping concentration and exact synthesis conditions, although not in a straightforward fashion.

Finally, we may remark that the impact of the quenching activity of IVCT states on the phosphor performance can be substantial even when relatively few mixed valence pairs are present. This is so because, even for low doping concentrations, energy can be transferred between Eu^{2+} ions, on the one hand, and thermal IVCT makes the distribution of Eu^{2+}/Eu^{3+} pairs across the sample dynamic, on the other, altogether making the IVCT non-radiative decay path virtually accessible to all Eu^{2+} ions. Nonradiative IVCT decay can hence be a microscopic explanation for concentration quenching. As an example, a study of the blue phosphor $BaMgAl_{10}O_{17}$:Eu showed that oxidation of only a small part of Eu^{2+} has a much more severe effect on the luminescence efficiency than one would expect from the decreasing Eu^{2+} content.[32]

Table 2: Properties of the experimentally found IVCT absorption bands for Eu in the alkaline earth fluorides. For comparison, theoretical results are given in second rows in bold font.

	CaF_2	SrF_2	BaF_2
Band maximum, λ_{max}^{IVCT} (nm)	562	430	337
Band maximum, E_{max}^{IVCT} (cm^{-1})	17791	23246	29702
	19300	**22500**	**26600**
Band FWHM, Γ^{IVCT} (cm^{-1})	5068	9235	(13375)
	7800	**8000**	**8200**
Relative absorption strength, $\frac{1-R(E_{max}^{IVCT})}{1-R(E_{max}^{fd})}$	0.03	0.08	0.11

In summary, we have provided direct evidence of IVCT states in multivalent lanthanide-doped hosts, which was missing, by combining their direct observation in diffuse reflectance spectra and their independent assignment with multiconfigurational *ab initio* calculations. We have shown their elusive nature (which made them largely overlooked so far) and, yet, their high potential to impact luminescence by quenching and excitation loss. The likely occurrence of IVCT states in other lanthanide-activated materials points out the importance of their study.

Theoretical and Experimental methods

The diabatic potential energy surfaces and electron transfer configurational diagrams for Eu^{2+}/Eu^{3+} mixed valence pair states were computed using the results of independent embedded cluster calculations as proposed in Refs. 19 and 20. The electronic structure of the donor $(EuF_8)^{6-}$ and acceptor $(EuF_8)^{5-}$ embedded clusters were obtained in two steps. In a first step, we used the spin-orbit-free many-electron relativistic second-order Douglas-Kroll-Hess (DKH) Hamiltonian[33,34] and, using the same type of basis set as in Ref. 20,[35,36] we performed state-average restricted-active-space self-consistent-field (SA-CASSCF)[37–39] calculations allowing all possible occupations in the Eu $4f$-shells and up to 4 electrons in the Eu $5f$, $5d$, and $6s$ shells; subsequent multi-state second-order perturbation theory (MS-CASPT2)[40–43] calculations allowed to correlate all cluster valence electrons. In the second step, we added the AMFI approximation of the DKH spin-orbit coupling operator to the Hamiltonian[44] and we performed restricted-active-space state-interaction spin-orbit (RASSI-SO)[45,46] calculations where all $(EuF_8)^{5-}$ $4f^6$ $2S+1$=7,5; all $(EuF_8)^{6-}$ $4f^7$ $2S+1$=8,6; and all $(EuF_8)^{6-}$ $4f^6(^7F_J)\times(5d,6s)$ $2S+1$=8 and $4f^6(^7F_J)\times 5de_g$ $2S+1$=6 states were allowed to interact. In all these calculations, the clusters were embedded in *ab initio* model potentials (AIMP)[47] that include Coulomb, exchange, and Pauli repulsion interactions from the CaF_2, SrF_2, and BaF_2 host lattices obtained in Ref. 20 from self-consistent embedded-ions (SCEI)[48] Hartree-Fock calculations and are available from the authors (see also Ref. 49). The suite of programs MOLCAS was used for all calculations.[49] The IVCT absorption band envelopes have been calculated using the time-dependent semiclassical approach of Heller[50,51] using the 21 electronic origins computed, the mean value of the totally symmetric vibrational frequency of the $4f^7$ and $4f^6$ ground states, their offset along the electron transfer reaction coordinate, an arbitrary value for the oscillator strenghts, and two different values for the widening factor.

Eu-doped (1 molar%) fluoride powders were prepared by a solid state synthesis, using fluoride precursors with a purity of at least 99%. Stoichiometric mixtures were fired at 800°C in a forming gas (10% H_2, 90% N_2) atmosphere. The phase purity of the resulting powders was verified by X-ray diffraction. Diffuse reflectance spectra were measured using a Varian Cary 500 spectrometer, equipped with an internal 110 mm $BaSO_4$ coated integrating sphere.

Acknowledgement This work was partially supported by Ministerio de Economía y Competitividad, Spain (Dirección General de Investigación y Gestión del Plan Nacional de I+D+i, MAT2014-54395-P and MAT2017-83553-P) and by the UGent Special Research Fund (BOF/PDO/2017/002101). The Fund for Scientific Research-Flanders (FWO) is acknowledged for a travel grant (V416818N).

References

(1) Verhoeven, J. W. Glossary of Terms Used in Photochemistry (IUPAC Recommendations 1996). *Pure Appl. Chem.* **1996**, *68*, 2223–2286.

(2) Marcus, R. A. Chemical and Electrochemical Electron-Transfer Theory. *Annu. Rev. Phys. Chem* **1964**, *15*, 155–196.

(3) Allen, G. C.; Hush, N. S. Intervalence-Transfer Absorption. Part 1. Qualitative Evidence for Intervalence-Transfer Absorption in Inorganic Systems in Solution and in the Solid State. *Prog. Inorg. Chem.* **1967**, *8*, 357–389.

(4) Robin, M.; Day, P. Mixed Valence Chemistry - A Survey and Classification. *Adv. Inorg. Chem. Radiochem.* **1968**, *10*, 247–422.

(5) Berkooz, O.; Malamud, M.; Shtrikman, S. Observation of Electron Hopping in $^{151}Eu_3S_4$ by Mössbauer Spectroscopy. *ssc* **1968**, *6*, 185–188.

(6) Wickleder, C. A New Mixed Valent Europium Chloride: $Na_5Eu_7Cl_{22}$. *Z. Naturforsch.* **2002**, *57b*, 901–907.

(7) Wickleder, C. KEu_2Cl_6 and $K_{1.6}Eu_{1.4}Cl_5$: Two New Mixed-Valent Europium Chlorides. *Z. Anorg. Allg. Chem.* **2002**, *628*, 1815–1820.

(8) van Schaik, W.; Lizzo, S.; Smit, W.; Blasse, G. Influence of Impurities on the Luminescence Quantum Efficiency of (La,Ce,Tb)PO_4. *J. Electrochem. Soc.* **1993**, *140*, 216–222.

(9) Smet, P. F.; Parmentier, A. B.; Poelman, D. Selecting conversion phosphors for white light-emitting diodes. *J. Electrochem. Soc.* **2011**, *158*, R37–R54.

(10) Smet, P. F.; Joos, J. J. White light-emitting diodes: Stabilizing colour and intensity. *Nat. Mater.* **2017**, *16*, 500–501.

(11) Kim, Y. H.; Arunkumar, P.; Kim, B. Y.; Unithrattil, S.; Kim, E.; Moon, S. H.; Hyun, J. Y.; Kim, K. H.; Lee, D.; Lee, J. S. et al. A zero-thermal-quenching phosphor. *Nat. Mater.* **2017**, *16*, 543–550.

(12) Martin, L. I. D. J.; Poelman, D.; Smet, P. F.; Joos, J. J. Microscopic Study of Dopant Distribution in Europium Doped $SrGa_2S_4$: Impact on Thermal Quenching and Phosphor Performance. *ECS J. Solid State Sci. Technol.* **2018**, *7*, R3052–R3056.

(13) Qiao, J. W.; Ning, L. X.; Molokeev, M. S.; Chuang, Y. C.; Liu, Q. L.; Xia, Z. G. Eu^{2+} Site Preferences in the Mixed Cation $K_2BaCa(PO_4)_2$ and Thermally Stable Luminescence. *J. Amer. Chem. Soc.* **2018**, *140*, 9730–9736.

(14) Bierwagen, J.; Yoon, S.; Gartmann, N.; Walfort, B.; Hagemann, H. Thermal and concentration dependent energy transfer of Eu^{2+} in $SrAl_2O_4$. *Opt. Mater. Express* **2016**, *6*, 793–803.

(15) Van der Heggen, D.; Joos, J. J.; Smet, P. F. Importance of Evaluating the Intensity Dependency of the Quantum Efficiency: Impact on LEDs and Persistent Phosphors. *ACS Photonics* **2018**, *5*, 4529–4537.

(16) Finley, E.; Tehrani, A. M.; Brgoch, J. Intrinsic Defects Drive Persistent Luminescence in Monoclinic $SrAl_2O_4$:Eu^{2+}. *J. Phys. Chem. C* **2018**, *122*, 16309–16314.

(17) Barandiarán, Z.; Meijerink, A.; Seijo, L. Configuration Coordinate Energy Level Diagrams of Intervalence and Metal-to-Metal Charge Transfer States of Dopant Pairs in Solids. *Phys. Chem. Chem. Phys.* **2015**, *17*, 19874–19884.

(18) Shannon, R. D. Revised Effective Ionic Radii and Systematic Studies of Interatomic Distances in Halides and Chalcogenides. *Acta Crystallogr. A* **1976**, *32*, 751–767.

(19) Seijo, L.; Barandiarán, Z. Intervalence Charge Transfer Luminescence: The Anomalous Luminescence of Ce-Doped $Cs_2LiLuCl_6$ Elpasolite. *J. Chem. Phys.* **2014**, *141*, 214706/1–214706/14.

(20) Barandiarán, Z.; Seijo, L. Intervalence Charge Transfer Luminescence: Interpaly Between Anomalous and $5d-4f$ Emissions in Yb-Doped Florite-Type Crystals. *J. Chem. Phys.* **2014**, *141*, 234704.

(21) Strek, W.; Tomala, R.; Marciniak, L.; Lukaszewicz, M.; Cichy, B.; Stefanski, M.; Hreniak, D.; Kedziorski, A.; Krosnicki, M.; Seijo, L. Broadband anti-Stokes white emission of Sr_2CeO_4 nanocrystals induced by laser irradiation. *Phys. Chem. Chem. Phys.* **2016**, *18*, 27921–27927.

(22) MacKeen, C.; Bridges, F.; Kozina, M.; Mehta, A.; Reid, M. F.; Wells, J.-P. R.; Barandiarán, Z. Evidence That the Anomalous Emission from CaF_2:Yb^{2+} Is Not Described by the Impurity Trapped Exciton Model. *J. Phys. Chem. Lett.* **2017**, *8*, 3313–3316.

(23) MacKeen, C.; Bridges, F.; Seijo, L.; Barandiarán, Z.; Kozina, M.; Mehta, A.; Reid, M. F.; Wells, J.-P. R. The Complexity of the CaF_2:Yb System: A Huge, Reversible, X-ray-Induced Valence Reduction. *J. Phys. Chem. C* **2017**, *121*, 28435–28442.

(24) Kaplyanskii, A. A.; Feofilov, P. P. The spectra of divalent rare earth ions in crystals of alkaline earth fluorides. II. Europium and Ytterbium. *Opt. Spectrosc.* **1962**, *13*, 129–132.

(25) Hong, B.; Kawano, K. Syntheses of Eu-Activated Alkaline Earth Fluoride MF_2 (M = Ca, Sr) Nanoparticles. *Japanese Journal of Applied Physics* **2007**, *46*, 6319–6323.

(26) Loh, E. $4f^n \rightarrow 4f^{n-1}5d$ Spectra of Rare-Earth Ions in Crystals. *Phys. Rev.* **1968**, *175*, 533.

(27) Moine, B.; Pédrini, C.; Courtois, B. Photoionization and Luminescences in BaF_2-Eu^{2+}. *J. Lumin.* **1991**, *50*, 31–38.

(28) Kubelka, P.; Munk, F. Ein Beitrag zur Optik der Farbanstriche. *Z. Tech. Phys.* **1931**, *12*, 8.

(29) Torrent, J.; Barrón, V. In *Methods of Soil Analysis: Mineralogical methods*; Ulery, A. L., Drees, L. R., Eds.; Soil Science Society of America, 2008; Chapter 13.

(30) Joos, J. J.; Poelman, D.; Smet, P. F. Energy level modeling of lanthanide materials: review and uncertainty analysis. *Phys. Chem. Chem. Phys.* **2015**, *17*, 19058–19078.

(31) Temme, N. M. In *NIST Handbook of Mathematical Functions*; Olver, F. W. J., Lozier, D. W., Boisvert, R. F., Clark, C. W., Eds.; Cambridge University Press, 2010; Chapter 7.

(32) Amidani, L.; Korthout, K.; Joos, J. J.; van der Linden, M.; Sijbom, H. F.; Meijerink, A.; Poelman, D.; Smet, P. F.; Glatzel, P. Oxidation and Luminescence Quenching of Europium in $BaMgAl_{10}O_{17}$ Blue Phosphors. *Chem. Mater.* **2017**, *29*, 10122–10129.

(33) Douglas, M.; Kroll, N. M. Quantum Electrodynamical Corrections to the Fine Structure of Helium. *Ann. Phys. (N.Y.)* **1974**, *82*, 89–155.

(34) Hess, B. A. Relativistic Electronic-Structure Calculations Employing a Two-Component No-Pair Formalism with External-Field Projection Operators. *Phys. Rev. A* **1986**, *33*, 3742–3748.

(35) Roos, B. O.; Lindh, R.; Malmqvist, P. A.; Veryazov, V.; Widmark, P. O. Main Group Atoms and Dimers Studied with a New Relativistic ANO Basis Set. *J. Phys. Chem. A* **2004**, *108*, 2851–2858.

(36) B. O. Roos, R. Lindh, P. A. Malmqvist, V. Veryazov, P. O. Widmark,; Borin, A. C. New Relativistic Atomic Natural Orbital Basis Sets for Lanthanide Atoms with Applications to the Ce Diatom and LuF_3. *J. Phys. Chem. A* **2008**, *112*, 11431–11435.

(37) Roos, B. O.; Taylor, P. R.; Siegbahn, P. E. M. A Complete Active Space SCF Method (CASSCF) Using a Density-Matrix Formulated Super-CI Approach. *Chem. Phys.* **1980**, *48*, 157–173.

(38) Siegbahn, P. E. M.; Heiberg, A.; Roos, B. O.; Levy, B. Comparison of the Super-CI and the Newton-Raphson Scheme in the Complete Active Space SCF Method. *Phys. Scr.* **1980**, *21*, 323–327.

(39) Siegbahn, P. E. M.; Heiberg, A.; Almlöf, J.; Roos, B. O. The Complete Active Space SCF (CASSCF) Method in a Newton-Raphson Formulation with Application to the HNO Molecule. *J. Chem. Phys.* **1981**, *74*, 2384–2396.

(40) Andersson, K.; Malmqvist, P.-A.; Roos, B. O.; Sadlej, A. J.; Wolinski, K. Second-Order Perturbation Theory with a CASSCF Reference Function. *J. Phys. Chem.* **1990**, *94*, 5483–5488.

(41) Andersson, K.; Malmqvist, P.-A.; Roos, B. O. Second-Order Perturbation Theory with a Complete Active Space Self-Consistent Field Reference Function. *J. Chem. Phys.* **1992**, *96*, 1218–1226.

(42) Zaitsevskii, A.; Malrieu, J.-P. Multi-Partitioning Quasidegenerate Perturbation Theory. A New Approach to Multireference Møller-Plesset Perturbation Theory. *Chem. Phys. Lett.* **1995**, *233*, 597–604.

(43) Finley, J.; Malmqvist, P.-A.; Roos, B. O.; Serrano-Andrés, L. The Multi-State CASPT2 Method. *Chem. Phys. Lett.* **1998**, *288*, 299–306.

(44) Hess, B. A.; Marian, C. M.; Wahlgren, U.; Gropen, O. A Mean-Field Spin-Orbit Method Applicable to Correlated Wavefunctions. *Chem. Phys. Lett.* **1996**, *251*, 365–371.

(45) Malmqvist, P. A.; Roos, B. O.; Schimmelpfennig, B. The RASSI Approach with Spin-Orbit Coupling. *Chem. Phys. Lett.* **2002**, *357*, 230–240.

(46) Paulovic, J.; Nakajima, T.; Hirao, K.; Lindh, R.; Malmqvist, P.-A. Relativistic and Correlated Calculations on the Ground and Excited States of ThO. *J. Chem. Phys.* **2003**, *119*, 798–805.

(47) Barandiarán, Z.; Seijo, L. The Ab Initio Model Potential Representation of the Crystalline Environment. Theoretical Study of the Local Distortion on NaCl:Cu^+. *J. Chem. Phys.* **1988**, *89*, 5739–5746.

(48) Seijo, L.; Barandiarán, Z. Ab Initio Model Potential Study of Local Distortions Around Cr^+ and Cr^{3+}. *J. Chem. Phys.* **1991**, *94*, 8158.

(49) Karlström, G.; Lindh, R.; Malmqvist, P. A.; Roos, B. O.; Ryde, U.; Veryazov, V.; Widmark, P. O.; Cossi, M.; Schimmelpfennig, B.; Neogrady, P. et al. MOLCAS: A Program Package for Computational Chemistry. *Comput. Mater. Sci.* **2003**, *28*, 222–239.

(50) Heller, E. J. Time-Dependent Approach to Semiclassical Dynamics. *J. Chem. Phys.* **1975**, *62*, 1544.

(51) Heller, E. J. The Semiclassical Way to Molecular Spectroscopy. *Acc. Chem. Res.* **1981**, *14*, 368.